The Journal of Chemical Physics

RESEARCH ARTICLE | SEPTEMBER 19 2024

GW with hybrid functionals for large molecular systems FREE

Tucker Allen ; Minh Nguyen ; Daniel Neuhauser

J. Chem. Phys. 161, 114116 (2024)
https://doi.org/10.1063/5.0219839

AIP Publishing

The Journal of Chemical Physics ARTICLE pubs.aip.org/aip/jcp

GW with hybrid functionals for large molecular systems

Cite as: J. Chem. Phys. 161, 114116 (2024); doi: 10.1063/5.0219839
Submitted: 20 May 2024 • Accepted: 5 September 2024 •
Published Online: 19 September 2024

Tucker Allen,[a] Minh Nguyen, and Daniel Neuhauser

AFFILIATIONS

Department of Chemistry and Biochemistry, University of California, Los Angeles, Los Angeles, California 90095, USA

[a]Author to whom correspondence should be addressed: tuckerallen27@ucla.edu

ABSTRACT

A low-cost approach for stochastically sampling static exchange during time-dependent Hartree–Fock-type propagation is presented. This enables the use of an excellent hybrid density functional theory (DFT) starting point for stochastic GW quasiparticle energy calculations. Generalized Kohn–Sham molecular orbitals and energies, rather than those of a local-DFT calculation, are used for building the Green function and effective Coulomb interaction. The use of an optimally tuned hybrid diminishes the starting point dependency in one-shot stochastic GW, effectively avoiding the need for self-consistent GW iterations.

I. INTRODUCTION

Kohn–Sham density functional theory (DFT) with local and semi-local functionals has been successful in calculating ground state energies and configurations but is insufficient for processes that involve excited states, such as (inverse) photoemission spectroscopy, as it gives too small bandgaps and incorrect quasiparticle (QP) energies.[1] An established alternative is the GW approximation to many-body perturbation theory (MBPT) for *ab initio* description of QPs.[2–4]

The GW method approximates the single-particle self-energy, which contains all many-body effects, as $\Sigma \approx iGW$, where G is the Green function that gives the probability amplitude of a QP to propagate between two space-time points and W is the screened Coulomb interaction. Common implementations of GW perturbatively correct the mean-field orbital energies, providing significant improvements; however, the method's perturbative nature yields observables that strongly depend on the initial set of mean-field orbitals and energies.[5,6] Therefore, Hedin's GW equations should ideally be solved iteratively.[7]

Neglecting the vertex function, the GW method begins with the noninteracting Green function, G_0, built with mean-field orbitals, and then one computes the screened interaction W with these same orbitals to obtain the self-energy Σ. In fully self-consistent GW (sc-GW), the dressed Green function $G = G_0 + G_0\Sigma G$ is then self-consistently updated till convergence. In contrast, one-shot G_0W_0 avoids updating the Green function and uses the noninteracting form. The least costly form of partial self-consistency, eigenvalue self-consistent GW_0 (ev-GW_0), follows this framework of freezing W and only updating the eigenvalues entering G.[8,9]

Many groups have studied the performance of GW ranging from partial to full self-consistency.[10–13] Eigenvalue-only schemes improve G_0W_0 results, and QP (qs-GW) self-consistency can fully remove the starting point dependency in the QP energies.[14,15] The qs-GW method approximates the dynamical non-Hermitian self-energy $\Sigma(\omega)$ with a static, non-local, and Hermitian operator. A low-scaling qs-GW well suited for molecules has been developed by Förster and co-workers.[16,17]

Recent work has found that a faithful description of molecular ionization potentials (IPs) can be achieved with sc-GW.[18] Spectral properties of finite systems tend to also improve with self-consistency.[19] Furthermore, sc-GW gives access to thermodynamic quantities, including the total ground state energy, electronic density, and equilibrium bond lengths.[19–21] However, iteratively solving the Dyson equation in a self-consistent field procedure often requires at least an order of magnitude increase in the computational cost of a G_0W_0 calculation.

For molecular systems with hundreds to thousands of electrons, a more realistic strategy is to improve the mean-field starting point within G_0W_0. For accurate frontier QP energies, long-range corrected (LC) hybrid functional DFT starting point G_0W_0 performs at least as well as the various types of self-consistency. Among local, semi-local, global, and RSH-DFT starting points, the use of an optimally tuned (OT)-RSH-DFT starting point has been shown

to give the lowest mean absolute errors (MAEs) relative to high-quality CCSD(T) values for the first IPs of the GW100 family of molecules.[22,23] Furthermore, OT hybrid starting point G_0W_0 has been shown to give excellent first electron affinities (EAs) and HOMO–LUMO gaps, even when rivaled against more intensive static second-order screened exchange (SOSEX) and fully dynamic G_3W_2 methods.[24] (For the remainder of this paper, the terms OT-RSH-DFT and hybrid DFT are used interchangeably.)

We have developed an efficient hybrid DFT method utilizing sparse-stochastic compression of the exchange kernel.[25] [Note that sparse-stochastic compression was first developed for stochastic GW (sGW) to reduce memory costs associated with time-ordering the retarded effective interaction W^R.[26–28]] For hybrid DFT, the exchange kernel is fragmented in momentum space with the vast majority of wave-vectors k represented through a small basis of sparse-stochastic vectors, except for a small fixed number of long-wavelength (low-k) components that are evaluated deterministically. These hybrid eigenstates, energies, and Hamiltonian serve as the DFT starting point of the present method.

Fully stochastic OT-RSH-DFT was previously used as an alternative to GW for frontier QP energies of large silicon nanocrystals.[29] We also developed a tuning procedure for OT hybrids to reproduce the GW fundamental bandgaps of periodic solids.[30] The present hybrid DFT starting point has very tiny stochastic error and differs from previous stochastic methods by avoiding stochastic sampling of the orbitals or density matrix.

In this article, sGW is extended to hybrid functional starting points. The sGW algorithm is briefly reviewed, and we emphasize specific parts of the method that have been modified for employing hybrid rather than local exchange–correlation (XC) functionals. In addition, we implement a "cleaning" procedure during time-propagation to avoid numerical instabilities, as we have recently done in generating a stochastic W for Bethe–Salpeter equation (BSE) spectra.[31,32] As demonstrated in Ref. 33, stochastic fluctuations worsen for hybrid DFT (compared to local/semi-local XC) starting-point G_0W_0 calculations because of the added sampling of the static exchange. The cleaning procedure significantly reduces the stochastic error in QP energies and enables routine hybrid starting-point G_0W_0 for molecular systems with thousands of valence electrons. The new approach is tested on a set of molecules with an OT-RSH functional. For technical details of the sGW method, we refer to Refs. 26–28.

II. THEORY

The stochastic paradigm for G_0W_0 uses the space-time representation of the single-particle self-energy,

$$\Sigma(r,r',t) = iG_0(r,r',t)W_0(r,r',t^+), \tag{1}$$

which takes a simple direct product form of the noninteracting single-particle Green function G_0 and screened Coulomb interaction W_0. In Sec. II A, we provide a stochastic form of G_0 and formulate how to obtain QP energies with a hybrid DFT basis. The sampling of static exchange during propagation of the Green function is also discussed.

It is convenient to split the self-energy as $\Sigma = \Sigma_X + \Sigma_P$, with an instantaneous Fock exchange part and time-dependent polarization part, respectively. To minimize the stochastic error of QP energies obtained with the sGW method, the Fock exchange contribution Σ_X to the self-energy is evaluated deterministically, while Σ_P is evaluated by a stochastic linear-response time-dependent Hartree propagation (sTDH),[26] equivalent to the standard random phase approximation (RPA). In Sec. II B, the sTDH approach is presented and we introduce a new projection routine that reduces statistical fluctuations when evaluating the action of W_0 on a source term.

A. Stochastic GW in space-time domain

1. Single-particle Green's function

In sGW, the single-particle Green function is converted to a random averaged correlation function. We first define the operator form of the zero-order Generalized Kohn–Sham (GKS) Green function,

$$iG_0(t) = e^{-iH_0t}[(I-P)\theta(t) - P\theta(-t)], \tag{2}$$

where I is the identity matrix and $P = \sum_{n\le N_{occ}} |\phi_n\rangle\langle\phi_n|$ projects onto the occupied subspace of the ground state GKS Hamiltonian,

$$H_0 = -\frac{1}{2}\nabla^2 + v_{e-N} + v_H[n_0] + v_{XC}^{\gamma}[n_0] + X^{\gamma}[\rho_0]. \tag{3}$$

Assuming closed-shell systems, the static density matrix is

$$\rho_0(r,r') = 2\sum_{n\le N_{occ}} \phi_n(r)\phi_n^*(r'), \tag{4}$$

and the diagonal elements yield the density $n_0(r) = \rho_0(r,r'=r)$. H_0 includes the kinetic energy, overall electron-nuclear potential, Hartree potential, exchange–correlation potential, and long-range exact exchange. The range-separation parameter γ divides the exchange interaction into short- and long-range components. For the short-range part, a local (or semi-local) exchange energy is used, while for the long-range part, a parameterized exact exchange operator is used.[34,35] The range-separation parameter is optimally tuned to each system of interest, and the tuning procedure enforces the ionization potential theorem of DFT.[36]

Stochastic projection onto the occupied and unoccupied subspaces of the GKS Hamiltonian (as in Refs. 9 and 28) requires a complete orthogonal basis to be defined on the grid. An approximate stochastic resolution of the identity (ROI)[37] is composed of N_ζ vectors, where each vector has a random signed value of $\zeta(r) = \pm 1/\sqrt{dV}$ at every grid-point, in which dV is the volume element. Statistical averaging of these N_ζ vectors produces $\{\zeta(r)\zeta(r')\}_\zeta = \delta_{r,r'}/dV = \delta(r-r')$, where the first and second delta symbols refer, respectively, to the Kronecker and Dirac delta functions. The N_ζ vectors thus make an approximate identity matrix $\mathcal{I} \simeq \frac{1}{N_\zeta}\sum_\zeta |\zeta\rangle\langle\zeta|$, which is exact in the limit $N_\zeta \to \infty$.

Inserting this identity to Eq. (2) produces

$$G_0(r,r',t) \simeq \frac{1}{N_\zeta}\sum_\zeta \tilde{\zeta}(r,t)\zeta^*(r'), \tag{5}$$

where $\tilde{\zeta}(r,t)$ is divided into positive and negative times corresponding to the propagation of electrons and holes,

$$\tilde{\zeta}(r,t) \equiv \begin{cases} \langle r|e^{-iH_0t}P|\zeta\rangle, & t<0, \\ \langle r|e^{-iH_0t}(I-P)|\zeta\rangle, & t>0. \end{cases}$$

In contrast to deterministic methods where exact eigenstates are evolved in time, a stochastic evaluation of the Green function requires propagation of randomly projected states; this makes the extension to hybrid functional starting points non-trivial. We discuss how to efficiently apply $X^\gamma[\rho_0]$ at each time step in Sec. II A 3.

To summarize, the stochastic ROI converts G_0 to a stochastic correlation function. Insertion of the N_ζ vectors enables a nested stochastic sampling procedure where, for every ζ (which samples the Green function), one defines an additional set of $\{\eta_l | l = 1, \ldots, N_\eta\}$ stochastic occupied orbitals for the sTDH propagation to obtain the polarization self-energy $\Sigma_P(t)$, detailed in Sec. II B 1.

2. QP energies with hybrid functionals

The input GKS MOs and energies fulfill $H_0\phi_j = \varepsilon_j\phi_j$. In this section, the GKS orbital energy is expressed as a sum of three parts,

$$\varepsilon \equiv \langle\phi|H_{\text{non-xc}} + v_{\text{XC}}^\gamma + X^\gamma|\phi\rangle, \tag{6}$$

where

$$H_{\text{non-xc}} = -\frac{1}{2}\nabla^2 + v_{\text{e-N}} + v_{\text{H}}[n_0]. \tag{7}$$

In a one-shot calculation, the diagonal GW QP energy is then perturbatively evaluated as

$$\varepsilon^{\text{QP}} = \langle\phi|H_{\text{non-xc}} + \Sigma_{\text{X}} + \Sigma_{\text{P}}(\omega = \varepsilon^{\text{QP}})|\phi\rangle, \tag{8}$$

where Σ_X is the Fock exchange self-energy operator with diagonal element for orbital ϕ,

$$\langle\phi|\Sigma_{\text{X}}|\phi\rangle = -\int \frac{\phi^*(r)\phi(r')}{|r-r'|}\rho_0(r,r')dr'dr, \tag{9}$$

and Σ_P is the polarization self-energy operator.

To avoid re-evaluating the approximate long-range exact exchange X^γ already done once in the hybrid DFT stage, we write

$$\varepsilon^{\text{QP}} = \varepsilon + \Delta, \tag{10}$$

where

$$\Delta = -\delta\varepsilon_0 + \langle\phi|\Sigma_{\text{X}} + \Sigma_{\text{P}}(\omega = \varepsilon^{\text{QP}})|\phi\rangle. \tag{11}$$

Here, $\delta\varepsilon_0 \equiv \varepsilon - \langle\phi|H_{\text{non-xc}}|\phi\rangle$ contains the approximate hybrid long-range exchange and short-range LDA XC potential from the GKS calculation.

3. Stochastic sampling of static exchange

The GKS Hamiltonian (including $X^\gamma[\rho_0]$) must be applied at every time step when acting with $G_0(t)$ and $W_0(t)$. Below, we detail the stochastic sampling for the Green function. This is done analogously for the sTDH stage. The action of the long-range exchange operator $X^\gamma[\rho_0]$ in the static H_0 is approximated very simply as

$$e^{-iX^\gamma dt} \approx C_{\text{norm}}(1 - iX^\gamma dt), \tag{12}$$

where C_{norm} is a normalization factor to conserve the norm of the propagated states. The action of $e^{-iX^\gamma dt}$ must be repeatedly evaluated at every time step, and to do this, we develop an improvement of earlier approaches. A previous approach to implement long-range explicit exchange starting points for sGW[33] sampled the same set of stochastic orbitals used for propagation, resulting in increased stochastic noise. This issue also appeared in early work on the stochastic BSE approach for optical spectra.[38]

To overcome these deficiencies, we first introduce an intermediate basis of N_β random functions,

$$\beta_\nu(r) = \sum_{i\in N_{occ}} a_{i\nu}\phi_i(r), \tag{13}$$

with coefficients

$$a_{i\nu} = \frac{1}{\sqrt{N_\beta}}e^{i\theta},\ \theta \in [0, 2\pi]. \tag{14}$$

The coefficients draw a random phase from the complex unit circle and give an equal amplitude for each ϕ_i orbital in the summation. These functions randomly scramble the information of the occupied subspace and give an approximate ground state density matrix,

$$p_0(r,r') \simeq \sum_{\nu\in N_\beta} \beta_\nu(r)\beta_\nu^*(r'). \tag{15}$$

We then prepare at every time step a *new* random vector,

$$b(r,t) = \sum_{\nu\in N_\beta} \pm\beta_\nu(r). \tag{16}$$

This vector is an instantaneous random linear combination of the finite β_ν functions that themselves stochastically sample the occupied space.

Since the exchange operator is time-independent, the β_ν functions do not need to be updated at every time step. This differs from previous stochastic TDHF (time-dependent Hartree–Fock) approaches where X^γ is based on $\rho(t)$ rather than ρ_0.[38] Sampling all the orbitals at every time step would be expensive, so we use this intermediate step of the β_ν functions. The required number of random occupied functions is quite small, with $N_\beta \approx 50$ used in this work. Convergence with this parameter is discussed in Sec. III.

Now, we are able to evaluate the action of the long-range exchange operator on an arbitrary state ψ,

$$\langle r|X^\gamma|\psi\rangle = -b(r,t)\int v_\gamma(|r-r'|)b^*(r',t)\psi(r')dr', \tag{17}$$

where $v_\gamma(|r-r'|) = \text{erf}(\gamma|r-r'|)/|r-r'|$ is the long-range exchange kernel. This stochastic sampling removes the sum over occupied states that appears when evaluating the action of exact exchange on a general ket.

B. Obtaining the polarization self-energy Σ_P

1. Stochastic TD-Hartree propagation

The polarization self-energy is evaluated on the real-time axis through the causal (retarded) linear response to an external test charge. Deterministically, this would be done through a time-dependent Hartree (TDH) propagation. However, TDH is prohibitive for large systems as one has to propagate all occupied orbitals. The stochastic approach circumvents this problem by perturbing and propagating a small number of orbitals that are each a

random linear combination of all occupied states. Here, we outline the parts of the sTDH propagation that relate to using an underlying GKS Hamiltonian. For a more detailed derivation of sTDH, we refer to Ref. 28.

For each vector ζ, we define a small set of $N_\eta (\approx 10-20)$ stochastic orbitals,

$$\eta_l(r) = \sum_{i \in N_{occ}} \eta_{il}\phi_i(r), \tag{18}$$

where $\eta_{il} = \pm 1$ and $\{\phi_i\}$ are the occupied GKS eigenfunctions. We emphasize that these η_{il} coefficients are different than the a_{iv} coefficients for sampling the static exchange. The use of numerically independent random bases helps avoid numerical bias in our results.

For orbital ϕ_n, computing the diagonal element of the polarization self-energy, $\langle\phi_n|\Sigma_P(t)|\phi_n\rangle$, requires that these stochastic occupied functions will be perturbed,

$$\eta_l^\lambda(r, t=0) = e^{-i\lambda v_{\text{pert}}}\eta_l(r), \tag{19}$$

with a Hartree-like potential $v_{\text{pert}}(r) \equiv \int |r-r'|^{-1}\zeta(r')\phi_n(r')dr'$, where λ is a perturbation strength $\approx 10^{-4}$ Ha^{-1}. These states are then evolved $\eta_l^\lambda(r, t+dt) = e^{-iH^\lambda(t)dt}\eta_l^\lambda(r,t)$ under the RPA (i.e., TDH) Hamiltonian,

$$H^\lambda(t) = H_0 + v_H[n^\lambda(t)] - v_H[n_0], \tag{20}$$

with the split-operator technique. Here, $n^\lambda(r,t) \equiv \frac{1}{N_\eta}\sum_l |\eta_l^\lambda(r,t)|^2$, and note that an additional set of unperturbed $\lambda = 0$ stochastic orbitals must also be propagated. From the potential difference, one obtains the retarded response,

$$u^R(r,t) = \frac{1}{\lambda}(v_H[n^\lambda(r,t)] - v_H[n^{\lambda=0}(r,t)]). \tag{21}$$

This time-dependent potential accounts for the variation in the Hartree field due to the introduction of a QP at $t = 0$.

The $u^R(r,t)$ potential [Eq. (21)] must first be time-ordered $u(r,t) = \mathcal{T}u^R(r,t)$ to yield the time-domain GW polarization self-energy,

$$\langle\phi_n|\Sigma_P(t)|\phi_n\rangle \approx \frac{1}{N_\zeta}\sum_\zeta \int \tilde{\zeta}(r,t)\phi_n(r)u(r,t)dr, \tag{22}$$

where $u(r,t)$ produces the action of the time-ordered effective interaction on the stochastic test charge,

$$u(r,t) = \int W_0(r,r',t)\zeta(r')\phi_n(r')dr'. \tag{23}$$

The time-ordering procedure uses the connection between time-ordered and retarded quantities in Fourier space.[26] Our previous work[28] reduces the memory costs of storing to disk $u^R(r,t)$ on every core, by using the sparse-stochastic compression sampling technique. All simulations in this work uses $N_\xi = 10\,000$ sparse vectors to time-order retarded quantities: $\langle\xi|u^R(t)\rangle \to \langle\xi|u(t)\rangle$. The $\Sigma_P(t)$ elements are then Fourier transformed to yield the polarization self-energy.

2. Orthogonality routine

Numerical instabilities during sTDH propagation may occur due to the contamination of the excited component $\eta_l^\lambda(t) - \eta_l^{\lambda=0}(t)$ by occupied state amplitudes. This artifact of the stochastic method is greatly alleviated by a method we introduced earlier in our BSE work (see Ref. 31), i.e., periodically "cleaning" the stochastic orbitals. More specifically, at every Mth time step, enforce orthogonality of the stochastic perturbed propagated states to all GKS occupied states by projecting onto the virtual subspace,

$$\eta_l^\lambda(t) \to \eta_l^{\lambda=0}(t) + (I-P)(\eta_l^\lambda(t) - \eta_l^{\lambda=0}(t)), \tag{24}$$

and then re-normalizing the "cleaned" $\eta_l^\lambda(t)$ vectors. For the present simulations, this projection is done every $M = 10$ time steps, where $dt = 0.05$, and the overall simulation time is 50 a.u. While previous implementations of sTDH in sGW propagated the $\eta_l^\lambda(t)$ and $\eta_l^{\lambda=0}(t)$ vectors separately, this added projection step requires now the simultaneous propagation of the two sets of states.

III. RESULTS

We test hybrid-sGW on various finite molecules, including urea, a series of polycyclic aromatic hydrocarbons, a model chlorophyll-a (Chla) monomer dye, and a hexamer photosynthetic dye complex found at the reaction center of photosystem II (RC-PSII).[39]

Table I shows the fundamental bandgaps for several approaches: local and hybrid DFT, stochastic GW based on an LDA starting point (one-shot and eigenvalue-iterative), and the present hybrid starting-point stochastic GW (one-shot and eigenvalue-iterative). The simplified eigenvalue-iterative stochastic GW, developed in Ref. 9, is denoted $\tilde{\Delta}GW_0$. The ionization potentials (IPs) of the same molecules are shown in Table II. The available reference values are provided for both the fundamental gaps and IPs.

Comparing the LDA and OT-RSH starting points, using the latter raises both the gap and IP by roughly 0.1–0.5 eV. We observe that, except for hexacene, the stand-alone hybrid-DFT eigenvalues serve as an excellent estimate for the IP and gap, as eigenvalue iterative $\tilde{\Delta}GW_0$ barely changes the results.

For the frontier QP energies of larger acenes, such as hexacene, it is well known[40] that both one-shot G_0W_0 and ev-GW schemes qualitatively differ from reference CCSD(T) estimates. In Ref. 33, only after the addition of a vertex correction was the LUMO QP energy for hexacene sufficiently increased so that the fundamental gap was in excellent agreement with the reference CCSD(T) values of Ref. 40.

The sGW calculations introduce correlation via Σ_P, which lowers the IPs and gaps of the acenes. However, for urea and the dye systems, the sGW IPs and gaps are slightly raised relative to the hybrid-DFT.

Figure 1 shows convergence of the IP of naphthalene, tetracene, and hexacene with respect to the number of N_β intermediate-exchange stochastic functions. These are used to sample the action of $X^\gamma[\rho_0]$ on all occupied states during orbital propagation. Going beyond $N_\beta = 50$ has minimal effect on the HOMO, and the overall error in the HOMO energy barely changes with N_β. We have verified

TABLE I. Fundamental bandgaps (in eV) using LDA- and hybrid-DFT starting points (with associated γ) with associated statistical error for various molecules. The literature CCSD(T) values for oligoacenes are from Ref. 40. The ev-*GW* fundamental bandgaps for the Chla monomer and the RC-PSII hexamer are from Ref. 39, which uses a modified version of the ADF 2022 software.[41]

Molecule	γ (bohr^{-1})	LDA-DFT	LDA + sGW	LDA + $\bar{\Delta}$GW$_0$	Hybrid-DFT	Hybrid + sGW	Hybrid + $\bar{\Delta}$GW$_0$	References
Urea	0.380	4.66	9.40 (0.07)	10.39 (0.07)	10.32	10.58(0.03)	10.61 (0.03)	
Naphthalene	0.285	3.34	7.60 (0.05)	7.97 (0.05)	8.63	8.47 (0.04)	8.46 (0.04)	8.73
Tetracene	0.220	1.63	5.07 (0.03)	5.35 (0.03)	5.82	5.73 (0.04)	5.72 (0.04)	6.14
Hexacene	0.200	0.57	3.46 (0.05)	3.66 (0.05)	4.26	4.05 (0.04)	4.04 (0.04)	4.85
Chla	0.160	1.40	3.73 (0.06)	3.88 (0.06)	4.37	4.22 (0.04)	4.21 (0.04)	4.41
RC-PSII	0.120	1.23	3.82 (0.05)	3.97 (0.05)	3.82	3.98 (0.05)	4.00 (0.05)	4.17

TABLE II. Ionization potentials (in eV) of finite molecules, taken as $I = -\varepsilon^{\mathrm{QP}}_{\mathrm{HOMO}}$, with statistical error of HOMO QP energy. Experimental values for urea and Chla are from Refs. 42 and 43, respectively. High-quality CCSD(T) values for acenes are from Ref. 40.

Molecule	LDA + sGW	LDA + $\bar{\Delta}$GW$_0$	Hybrid-DFT	Hybrid + sGW	Hybrid + $\bar{\Delta}$GW$_0$	References
Urea	9.35 (0.07)	10.30 (0.07)	10.58	10.77 (0.05)	10.79 (0.05)	10.28
Naphthalene	8.21 (0.04)	8.44 (0.04)	8.68	8.66 (0.03)	8.63 (0.03)	8.25
Tetracene	7.03 (0.02)	7.22 (0.02)	7.37	7.36 (0.03)	7.36 (0.03)	6.96
Hexacene	6.23 (0.04)	6.38 (0.04)	6.59	6.50 (0.05)	6.49 (0.05)	6.32
Chla	6.42 (0.06)	6.58 (0.06)	6.68	6.69 (0.05)	6.70 (0.05)	6.1
RC-PSII	5.76 (0.05)	5.91 (0.05)	6.13	6.26 (0.05)	6.27 (0.05)	

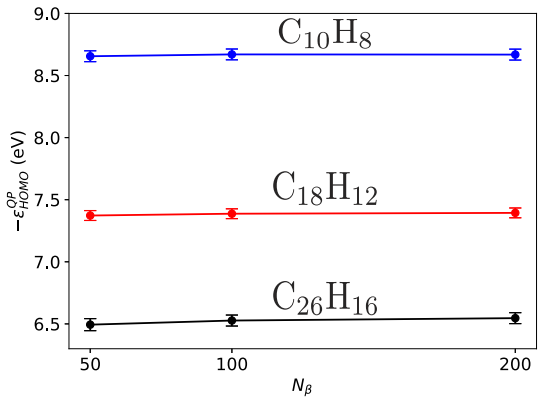

FIG. 1. Convergence of the ionization potential (IP) of linear acenes (hybrid-DFT + sGW) with respect to N_β, the number of intermediate stochastic functions for evaluating the static exchange [Eq. (13)].

for the RC-PSII, with $N_{occ} = 660$ occupied orbitals, that increasing N_β to 100 does not change the results.

Here, we review the added computational cost in using hybrid functional starting points for stochastic G_0W_0. Operation-wise, for each time step, preparing the vector $b(r,t)$ costs $N_\beta N_g$ operations and the evaluation of the static exchange requires $N_\eta N_g N_g$ operations, where N_g is the number of grid points. A technical point is that the convolutions in Eq. (17) use the Martyna–Tuckerman grid-doubling approach, so the computational effort is higher by an order of magnitude.[44]

We finally showcase the power of this stochastic framework by studying the 1320 valence electron RC-PSII. The reported OT-RSH-DFT starting point stochastic GW QP energies are converged within a statistical error of 0.05 eV using only $N_\zeta = 1024$ stochastic runs. Both the nuclear coordinates and reference atomic basis-set ev-GW energies for this system are from Ref. 39. The reference calculation uses the Perdew–Burke–Ernzerhof (PBE) global hybrid with 40% exact exchange and includes scalar relativistic effects. We obtain fairly good agreement (<0.2 eV discrepancy) between the reference ev-GW fundamental bandgap and one-shot sGW with an optimally tuned hybrid starting point. For this large complex, our tuned hybrid has a range-separation parameter of $\gamma = 0.12$ bohr^{-1}. This small value indicates *weak* long-range exchange, and it is reasonable that the sGW bandgap of RC-PSII obtained with this starting point is lower than with the global hybrid functional starting point (i.e., the global hybrid method opens the gap more than the tuned hybrid).

IV. CONCLUSIONS

We introduced an approach to efficiently sample static exchange during TDHF-type propagation. This general method is applied here to implement hybrid-DFT starting points to stochastic GW calculations. Our results use the long-range Baer–Neuhauser–Lifshitz (BNL) functional,[45] but the method is amenable to a wide range of hybrids; future studies will benchmark sGW with different hybrid-DFT starting points.

The stochastic sampling approach to evaluate long-range exchange during propagation of G_0 and W_0 is only $\approx$1.5 – 2 times more expensive than using an LDA starting point sGW. Because the long-range exchange operator functionally depends on the static density matrix, ρ_0, a stochastic sampling approach is the optimal choice as one can sample the occupied subspace only once.

The hybrid sGW gaps presented are quite close (usually within less than 0.5 eV) to the hybrid-DFT gaps, so eigenvalue self-consistency makes only a further minor difference in final bandgaps. One explanation is that the starting GKS energies correspond to a Hamiltonian with the same $-1/r$ asymptotic behavior in the exchange potential as the true GW Hamiltonian. This makes GKS energies a much better starting point for the GW perturbation expansion [Eq. (8)] than LDA energies that possess exponential decay in their exchange potential.

The hybrid-DFT frontier eigenvalues effectively mimic the GW HOMO and LUMO QP energies. This holds promise for studying neutral excitations in the stochastic GW-BSE (see Refs. 31 and 32), where the hybrid-DFT eigensystem will be used for the electron–hole exciton basis, rather than true QP orbitals and energies. This could avoid the need to perform GW corrections to DFT eigenvalues altogether, while having a minor impact on the resulting optical spectrum.

In future work, sparse-stochastic exchange will be applied to vertex corrections of the GW self-energy. Vertex corrections have been found to be important for accurate description of plasmons. More fundamentally, inclusion of an approximate non-local vertex can partially correct the self-screening introduced when computing the self-energy in the RPA.[46,47] It has been shown that a TDHF vertex provides a screened interaction W that is completely free of self-screening error.[48–50] Previous work on low-order stochastic approximations of the vertex function amounts to introducing a scaled non-local exchange term in the polarization part of the self-energy.[51–52] Our sparse-stochastic exchange technique with orbital-cleaning would efficiently tackle this calculation.

ACKNOWLEDGMENTS

Computational resources for simulations were provided by both the Expanse cluster at San Diego Supercomputer Center through allocation PHY220143 from the Advanced Cyberinfrastructure Coordination Ecosystem: Services & Support (ACCESS) program[53] and the resources of the National Energy Research Scientific Computing Center, a DOE Office of Science User Facility supported by the Office of Science of the U.S. Department of Energy under Contract No. DE-AC02-05CH11231 using NERSC Award No. BES-ERCAP0029462.

AUTHOR DECLARATIONS

Conflict of Interest

The authors have no conflicts to disclose.

Author Contributions

Tucker Allen: Conceptualization (equal); Data curation (equal); Formal analysis (equal); Investigation (equal); Methodology (equal); Software (equal); Validation (equal); Writing – original draft (equal); Writing – review & editing (equal). **Minh Nguyen**: Data curation (equal); Validation (equal). **Daniel Neuhauser**: Conceptualization (equal); Investigation (equal); Methodology (equal); Project administration (equal); Resources (equal); Software (equal); Supervision (equal); Writing – review & editing (equal).

DATA AVAILABILITY

The data that support the findings of this study are available from the corresponding author upon reasonable request.

REFERENCES

[1] J. P. Perdew, "Density functional theory and the band gap problem," Int. J. Quantum Chem. **28**(S19), 497–523 (1985).
[2] F. Aryasetiawan and O. Gunnarsson, "The ***GW*** method," Rep. Prog. Phys. **61**(3), 237 (1998).
[3] G. Onida, L. Reining, and A. Rubio, "Electronic excitations: Density-functional versus many-body Green's-function approaches," Rev. Mod. Phys. **74**, 601–659 (2002).
[4] L. Reining, "The GW approximation: Content, successes and limitations," Wiley Interdiscip. Rev.: Comput. Mol. Sci. **8**(3), e1344 (2018).
[5] L. Y. Isseroff and E. A. Carter, "Importance of reference Hamiltonians containing exact exchange for accurate one-shot ***GW*** calculations of Cu_2O," Phys. Rev. B **85**(23), 235142 (2012).
[6] F. Bruneval and M. A. L. Marques, "Benchmarking the starting points of the ***GW*** approximation for molecules," J. Chem. Theory Comput. **9**(1), 324–329 (2013).
[7] L. Hedin, "New method for calculating the one-particle Green's function with application to the electron-gas problem," Phys. Rev. **139**, A796–A823 (1965).
[8] A. Stan, N. E. Dahlen, and R. van Leeuwen, "Levels of self-consistency in the *GW* approximation," J. Chem. Phys. **130**(11), 114105 (2009).
[9] V. Vlcek, R. Baer, E. Rabani, and D. Neuhauser, "Simple eigenvalue-self-consistent ΔGW_0," J. Chem. Phys. **149**(17), 174107 (2018).
[10] X. Blase, C. Attaccalite, and V. Olevano, "First-principles ***GW*** calculations for fullerenes, porphyrins, phtalocyanine, and other molecules of interest for organic photovoltaic applications," Phys. Rev. B **83**, 115103 (2011).
[11] N. Marom, F. Caruso, X. Ren, O. T. Hofmann, T. Körzdörfer, J. R. Chelikowsky, A. Rubio, M. Scheffler, and P. Rinke, "Benchmark of *GW* methods for azabenzenes," Phys. Rev. B **86**, 245127 (2012).
[12] F. Bruneval and M. Gatti, *Quasiparticle Self-Consistent GW Method for the Spectral Properties of Complex Materials* (Springer, Berlin, Heidelberg, 2014), pp. 99–135.
[13] W. Chen and A. Pasquarello, "Band-edge positions in *GW*: Effects of starting point and self-consistency," Phys. Rev. B **90**, 165133 (2014).
[14] S. V. Faleev, M. van Schilfgaarde, and T. Kotani, "All-electron self-consistent *GW* approximation: Application to Si, MnO, and NiO," Phys. Rev. Lett. **93**, 126406 (2004).
[15] F. Kaplan, M. E. Harding, C. Seiler, F. Weigend, F. Evers, and M. J. van Setten, "Quasi-particle self-consistent *GW* for molecules," J. Chem. Theory Comput. **12**(6), 2528–2541 (2016).
[16] A. Förster and L. Visscher, "Low-order scaling quasiparticle self-consistent GW for molecules," Front. Chem. **9** (2021).
[17] A. Förster, E. van Lenthe, E. Spadetto, and L. Visscher, "Two-component *GW* calculations: Cubic scaling implementation and comparison of vertex-corrected and partially self-consistent *GW* variants," J. Chem. Theory Comput. **19**(17), 5958–5976 (2023).
[18] M. Wen, V. Abraham, G. Harsha, A. Shee, K. B. Whaley, and D. Zgid, "Comparing self-consistent *GW* and vertex-corrected G_0W_0 ($G_0W_0\Gamma$) accuracy for molecular ionization potentials," J. Chem. Theory Comput. **20**(8), 3109–3120 (2024).
[19] F. Caruso, P. Rinke, X. Ren, A. Rubio, and M. Scheffler, "Self-consistent *GW*: All-electron implementation with localized basis functions," Phys. Rev. B **88**, 075105 (2013).
[20] B. Holm and U. von Barth, "Fully self-consistent **GW** self-energy of the electron gas," Phys. Rev. B **57**, 2108–2117 (1998).

[21]C. Di Valentin, S. Botti, and M. Cococcioni, *First Principles Approaches to Spectroscopic Properties of Complex Materials* (Springer, Berlin, Heidelberg, 2014).
[22]S. E. Gant, J. B. Haber, M. R. Filip, F. Sagredo, D. Wing, G. Ohad, L. Kronik, and J. B. Neaton, "Optimally tuned starting point for single-shot ***GW*** calculations of solids," Phys. Rev. Mater. **6**, 053802 (2022).
[23]C. A. McKeon, S. M. Hamed, F. Bruneval, and J. B. Neaton, "An optimally tuned range-separated hybrid starting point for *ab initio* GW plus Bethe–Salpeter equation calculations of molecules," J. Chem. Phys. **157**(7), 074103 (2022).
[24]F. Bruneval and A. Förster, "Fully dynamic *G*3*W*2 self-energy for finite systems: Formulas and benchmark," J. Chem. Theory Comput. **20**(8), 3218–3230 (2024).
[25]N. C. Bradbury, T. Allen, M. Nguyen, and D. Neuhauser, "Deterministic/fragmented-stochastic exchange for large-scale hybrid DFT calculations," J. Chem. Theory Comput. **19**(24), 9239–9247 (2023).
[26]D. Neuhauser, Y. Gao, C. Arntsen, C. Karshenas, E. Rabani, and R. Baer, "Breaking the theoretical scaling limit for predicting quasiparticle energies: The stochastic ***GW*** approach," Phys. Rev. Lett. **113**(7), 076402 (2014).
[27]V. Vlček, E. Rabani, D. Neuhauser, and R. Baer, "Stochastic GW calculations for molecules," J. Chem. Theory Comput. **13**(10), 4997–5003 (2017).
[28]V. Vlček, W. Li, R. Baer, E. Rabani, and D. Neuhauser, "Swift ***GW*** beyond 10 000 electrons using sparse stochastic compression," Phys. Rev. B **98**, 075107 (2018).
[29]D. Neuhauser, E. Rabani, Y. Cytter, and R. Baer, "Stochastic optimally tuned range-separated hybrid density functional theory," J. Phys. Chem. A **120**(19), 3071–3078 (2016).
[30]W. Li, V. Vlcek, H. Eisenberg, E. Rabani, R. Baer, and D. Neuhauser, "Tuning the range separation parameter in periodic systems," arXiv:2102.11041 (2021).
[31]N. C. Bradbury, M. Nguyen, J. R. Caram, and D. Neuhauser, "Bethe–Salpeter equation spectra for very large systems," J. Chem. Phys. **157**(3), 031104 (2022).
[32]N. C. Bradbury, T. Allen, M. Nguyen, K. Z. Ibrahim, and D. Neuhauser, "Optimized attenuated interaction: Enabling stochastic Bethe–Salpeter spectra for large systems," J. Chem. Phys. **158**(15), 154104 (2023).
[33]V. Vlcek, "Stochastic vertex corrections: Linear scaling methods for accurate quasiparticle energies," J. Chem. Theory Comput. **15**(11), 6254–6266 (2019).
[34]T. Leininger, H. Stoll, H.-J. Werner, and A. Savin, "Combining long-range configuration interaction with short-range density functionals," Chem. Phys. Lett. **275**(3–4), 151–160 (1997).
[35]A. D. Becke, "Density-functional thermochemistry. III. The role of exact exchange," J. Chem. Phys. **98**(7), 5648–5652 (1993).
[36]R. Baer, E. Livshits, and U. Salzner, "Tuned range-separated hybrids in density functional theory," Annu. Rev. Phys. Chem. **61**(1), 85–109 (2010).
[37]R. Baer, D. Neuhauser, and E. Rabani, "Self-averaging stochastic Kohn–Sham density-functional theory," Phys. Rev. Lett. **111**(10), 106402 (2013).
[38]E. Rabani, R. Baer, and D. Neuhauser, "Time-dependent stochastic Bethe–Salpeter approach," Phys. Rev. B **91**, 235302 (2015).
[39]A. Förster and L. Visscher, "Quasiparticle self-consistent *GW*-Bethe–Salpeter equation calculations for large chromophoric systems," J. Chem. Theory Comput. **18**(11), 6779–6793 (2022).
[40]T. Rangel, S. M. Hamed, F. Bruneval, and J. B. Neaton, "Evaluating the *GW* approximation with CCSD(T) for charged excitations across the oligoacenes," J. Chem. Theory Comput. **12**(6), 2834–2842 (2016).
[41]G. te Velde, F. M. Bickelhaupt, E. J. Baerends, C. Fonseca Guerra, S. J. A. van Gisbergen, J. G. Snijders, and T. Ziegler, "Chemistry with ADF," J. Comput. Chem. **22**(9), 931–967 (2001).
[42]D. J. Russell *et al.*, NIST computational chemistry comparison and benchmark database, http://srdata.nist.gov/cccbdb, 2006.
[43]N. Shafizadeh, M. H. Ha-Thi, B. Soep, M.-A. Gaveau, F. Piuzzi, and C. Pothier, "Spectral characterization in a supersonic beam of neutral chlorophyll a evaporated from spinach leaves," J. Chem. Phys. **135**, 114303 (2011).
[44]G. J. Martyna and M. E. Tuckerman, "A reciprocal space based method for treating long range interactions in *ab initio* and force-field-based calculations in clusters," J. Chem. Phys. **110**(6), 2810–2821 (1999).
[45]R. Baer and D. Neuhauser, "Density functional theory with correct long-range asymptotic behavior," Phys. Rev. Lett. **94**, 043002 (2005).
[46]P. Romaniello, S. Guyot, and L. Reining, "The self-energy beyond *GW*: Local and nonlocal vertex corrections," J. Chem. Phys. **131**, 154111 (2009).
[47]S. Di Sabatino, P.-F. Loos, and P. Romaniello, "Scrutinizing GW-based methods using the Hubbard dimer," Front. Chem. **9** (2021).
[48]E. Maggio and G. Kresse, "*GW* vertex corrected calculations for molecular systems," J. Chem. Theory Comput. **13**(10), 4765–4778 (2017).
[49]Y.-W. Chang and B.-Y. Jin, "Self-interaction correction to GW approximation," Phys. Scr. **86**(6), 065301 (2012).
[50]G. Rohringer, A. Valli, and A. Toschi, "Local electronic correlation at the two-particle level," Phys. Rev. B **86**(12), 125114 (2012).
[51]C. Mejuto-Zaera and V. Vlček, "Self-consistency in *GWT* formalism leading to quasiparticle-quasiparticle couplings," Phys. Rev. B **106**, 165129 (2022).
[52]G. Weng, R. Mallarapu, and V. Vlček, "Embedding vertex corrections in *GW* self-energy: Theory, implementation, and outlook," J. Chem. Phys. **158**(14), 144105 (2023).
[53]T. J. Boerner, S. Deems, T. R. Furlani, S. L. Knuth, and J. Towns, "ACCESS: Advancing innovation: NSF's advanced cyberinfrastructure coordination ecosystem: Services and support," in *Practice and Experience in Advanced Research Computing July 23–27, 2023, Portland, OR* (ACM, New York, 2023), pp. 173–176.